

Interactions of polarizable media in water: A molecular dynamics approach

A. Wynveen^{a)} and F. Bresme^{b)}*Department of Chemistry, Imperial College London, SW7 2AZ London, United Kingdom*

(Received 28 November 2005; accepted 24 January 2006; published online 9 March 2006)

We investigate the interactions of polarizable solutes in water as a function of the solute permittivity. A generic and computationally efficient simulation methodology for the investigation of systems involving dielectric discontinuities is introduced. We report results for interactions between two polarizable cylindrical solutes of nanometer dimensions, which demonstrate that the interactions between the solutes strongly depend on the solute permittivity ϵ . For low permittivity, $\epsilon \sim 1-2$, the interactions are dominated by surface tension forces whose origin lies in the formation of a vapor cavity between the two hydrophobic solutes. This effect leads to a drying transition, where the intersolute force changes discontinuously at a specific solute-solute separation. We find that a moderate permittivity, $\epsilon \sim 20$, enhances the solvation of the polarizable objects inhibiting this drying transition. In the limit of moderately high permittivity, the interactions are dominated by solvation forces. These forces are much larger than those calculated using macroscopic models of dielectrics, which consider water as a continuum dielectric medium. Our results emphasize the importance of including the solvent explicitly to investigate dielectric discontinuities and interactions between polarizable media in water. © 2006 American Institute of Physics. [DOI: 10.1063/1.2177244]

I. INTRODUCTION

The molecular description of solute polarizability is of great relevance to understand interfacial problems involving both inorganic-water and *in vivo* or *in vitro* biological-water interfaces. Computer simulations have shown that it is necessary to include the polarizability in order to adequately describe the relevant experiments. For example, models of polyelectrolytes¹ and colloidal spheres² near walls must include effects associated with the dielectric discontinuity at the solvent-wall interface to account for the behavior observed in experiments. At the simplest level, the interactions between dielectric media can be described by incorporating image charges to account for the dielectric discontinuity that exists between two different media.³ Such image charge models can make predictions, e.g., the discrepancy in forces between electrical double layers with different surface charges or adsorbed polar solutes,^{4,5} that cannot be obtained via mean field theories.

Understanding the role of water in solutions is critical for determining the interactions between neutral dielectric objects within the solution. When the solutes are at large separations (≥ 5 nm) and low concentrations ($\leq 0.01M$), water may be treated as a continuous dielectric medium (see, e.g., Ref. 6). At large solute concentrations or at narrow separations, however, these interactions necessarily become far more complicated due to the complex structure and properties of water. In fact, the molecular nature of water then becomes significant, giving rise to a dielectric response that differs from the one expected on macroscopic grounds.⁷ It is clear that in order to advance the description of the solute-

water interface, it is essential to develop a molecular description of the dielectric discontinuities involving water-solute interfaces.

Computational models of solutions with different dielectric media tend to incorporate solvation and other polarizability effects without treating the solvent explicitly, which vastly improves the computational efficiency of the simulations.⁸ Such continuum solvent models may make use of boundary element or reaction field methods of multiple dielectrics to account for inhomogeneities across these systems.⁹ There also exist simulation models where both the solvent and macroscopic dielectrics are treated as continuous media,¹⁰ in which the dielectric discontinuity is included through induced surface charges at the interfaces.¹¹ In order to describe phenomena in very confined geometries or at the surface itself, however, the use of an explicit solvent may be required.

In this article, we present a simple computational approach for treating generic polarizable media in an explicit solvent within molecular dynamics computer simulations. Part of our motivation lies in testing analytical models, e.g., that of interactions of helical macromolecules of a cylindrical shape,¹² that rely on continuum theories for water and other dielectric media. Within this model, we can analyze the influence of solute polarizability on the solvent structure as well as on the solute-solute interactions mediated by the solvent.

The paper is structured as follows. Section II describes the methodology used to model the solute polarizability. Details of the equations needed to implement the method are given in the Appendix. We use the method to investigate two problems: (i) the water structure around a single polarizable cylindrical solute as a function of the solute permittivity and (ii) the interactions between two polarizable cylinders in wa-

^{a)}Electronic mail: awynveen@imperial.ac.uk^{b)}Electronic mail: fbresme@imperial.ac.uk

ter. Our results indicate that the coupling between the solute polarizability and molecular nature of the solvent results in effects that cannot be predicted using continuum models. We conclude the paper with a discussion and some final remarks.

II. METHODOLOGY AND SIMULATION DETAILS

Molecular dynamics simulations were carried out for systems with one or two polarizable cylindrical objects in solution. A hydrophobic cylinder in solution was created in the molecular dynamics simulation by introducing an external repulsive potential of the form

$$V(r) = \left(\frac{\sigma}{r}\right)^n, \quad (1)$$

which, we assume, acts on *both* the hydrogen and oxygen atoms of the surrounding water. We set σ to be 9 Å and n is

$$\sigma_{\text{ind}}(R_c, \varphi, z) = \sum_{m=-\infty}^{\infty} e^{im\varphi} \int_0^{\infty} dk \frac{(\kappa-1)q}{2\pi^2 R_c} \frac{I'_m(kR_c)K_m(kd)}{[I_m(kR_c)K'_m(kR_c) - \kappa I'_m(kR_c)K_m(kR_c)]} \cos(kz). \quad (2)$$

Here, $\kappa = 1 + \chi = \epsilon_{\text{in}}/\epsilon_{\text{out}}$ is the ratio of the electric permittivity of the solute to that of the surrounding media. Since the water solvent is treated explicitly ϵ_{out} is set to unity.

The treatment of the effects of the polarizable solute in a molecular dynamics code involves computing the induced charge on the surface of the dielectric cylinder at every time step due to the external charge distribution given by the solvent. The computation is implemented by treating the induced surface charge as a series of point charges that are positioned on a grid that envelops the cylindrical surface.¹¹ These grid charges are easily included as fixed atoms in the molecular dynamics simulation. The charge magnitude of each grid point is given by Eq. (2). The grid points must be compact enough to avoid commensurability between the external charges and the grid and to preclude artifacts due to the grid geometry. Also, the grid must lie inside the surface defined by the repulsive potential [Eq. (1)] so that the external charges of the solution cannot collapse onto the grid charges. The results reported below were obtained using a square lattice grid, with spacing between grid points of 1 Å, and the grid was located at $R_c = 7$ Å. We found that these parameters are adequate for the present study.

In order that Eq. (2) need not be calculated for every external charge at each simulation time step, which would be very computationally time consuming, a lookup table is used to determine the magnitude of the grid charges due to an external charge distribution. This table, with indices corresponding to the distance of the external charge from the dielectric surface and the ϕ, z grid points on the dielectric surface, can be generated at the beginning of the simulation. For external charges lying in between two indices, a linear

taken to be 50, so that the object's surface is smooth but allows for ~ 1 Å penetration of the solvent molecules with $k_B T$ kinetic energy. Here, r is the radial distance (cylindrical coordinates) from the center of the cylinder to the oxygen and hydrogen atoms.

To model the finite polarizability of the object, we assume that the cylinder responds as a linear dielectric to applied fields. Therefore, there is a discontinuity in the electric field at the solute surface, generated by external charges. In our case the external charges are those of the explicit water molecules at the cylinder/solvent boundary. This dielectric discontinuity in the field is taken into account by defining an induced charge on the surface of the cylinder. As derived in the Appendix,¹³ the induced surface charge of a cylinder of radius R_c at the location (R_c, φ, z) due to an external point charge q that lies at $(r' = d (d > R_c), \varphi' = 0, z' = 0)$ is

interpolation is used to determine the magnitude of the grid charge at a specific location. In order to reduce the computational expense, only certain grid charges, i.e., those within ~ 10 Å from the point on the grid nearest the external charge, need to be considered. This approximation is justified since the amount of induced surface charge due to a given external charge decays very quickly when moving away from the point on the surface closest to the external charge. Of course this decay depends on the distance of the external charge from the surface. Charges farther away leave a broader distribution of surface charge. But external charges far away from the surface will have much less influence on the magnitude of the induced charge as compared to those charges near the surface. Finally, once the total grid charge is calculated, each grid charge is shifted in value by the average of the induced charge to maintain charge neutrality of the polarizable media.

A comparison between the exact solution for the induced potential [Eq. (A4)] and that found from using the grid charges is shown in Fig. 1. It shows that the method outlined above gives a good account of the exact potential due to the induced charge on the dielectric. Again, the simulation method does not involve an iterative method, which would be more computationally demanding. The small discrepancy with the exact potential arises from a combination of the discretization of the induced surface charge and of using a finite number of these discretized grid charges to model the induced charge on the dielectric media. Despite these simplifications our method results in electrostatic potentials that are in good agreement with the exact potential. Therefore, the method can be used to investigate in a systematic and com-

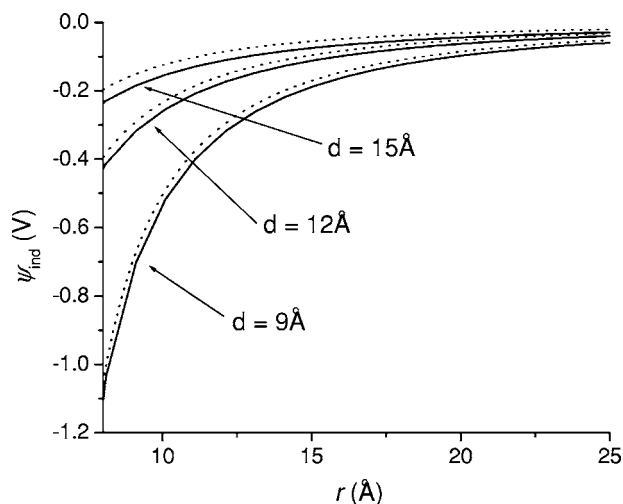


FIG. 1. The potential due to the induced charge on a dielectric cylinder ($\epsilon_{in}=2$, $R_c=7$ Å) arising from an external unit charge placed at different locations from the cylinder's axis [d in Eq. (2)]. The solid lines correspond to the exact solution [Eq. (A4)] whereas the dotted lines correspond to that calculated using the discrete grid charges [Eq. (2)] within ~ 10 Å of the point on the grid closest to the external charge. The potential is shown as a function of the position along the radial vector that passes through the external charge.

putationally inexpensive way the effects of the polarizability on the interactions between polarizable media in an explicit solvent.

When more than one polarizable object is considered, we compute the induced charge on one object, and then its charge configuration is used to compute the induced charge on another polarizable object. Upon calculation of the grid charges for a specific object, the values of the grid charges for that object are shifted by an equal amount, the average value of its grid charges, so that it possesses charge neutrality as is done when there is only one object. This entire process is iterated until convergence of the magnitude of each grid charge on all the objects is reached. Convergence typically requires only a few steps so that this calculation is computationally inexpensive.

In our simulations, the Simple Point Charge/Extended (SPC/E) water model was chosen over more involved polarizable models. It has been found that this rigid model yields very similar results to those obtained from more complex polarizable models; e.g., water next to hydrophobic surfaces,¹⁴ metal surfaces,¹⁵ and charged surfaces,¹⁶ as well as the liquid-vapor interface^{14,17} demonstrate that the structure of the water and the associated fields within the simulations were relatively independent of whether a polarizable or nonpolarizable model of water was used. Also, we have used the SPC/E model to investigate Newton Black Films, finding very good agreement with the available experimental data.¹⁸ Furthermore, using this rigid form of nonpolarizable water, which has very few degrees of freedom compared to polarizable models, greatly reduces the computational time of the simulations.

The SPC/E model consists of three charged sites. The charges on the oxygen and hydrogens are $q_O=-0.8476e$ and $q_H=-q_O/2$, respectively. The water geometry is defined by the oxygen-hydrogen bond length, 1 Å, and the HOH angle,

109.5°. In addition to electrostatic interactions, van der Waals interactions are modeled through the Lennard-Jones potential with parameters $\epsilon=0.6502$ kJ/mol and $\sigma=3.169$ Å.

The Coulombic interactions arising from the water-water, water-cylinder, and cylinder-cylinder interactions were computed using the three dimensional version of the Ewald summation method. The parameters for the Ewald sum were chosen to give a relative error in the computation of the Coulombic interactions of the order of 10^{-6} . In addition we considered “conducting” boundary conditions. Short-ranged interactions were cut off at 17 Å. The simulations were performed in the canonical (NVT) ensemble at a temperature $T=298$ K. A typical simulation consisted of >50 000 equilibration steps, which are discarded, and another >200 000 time steps for production. The time step in the simulations was 2 fs. The simulations reported below were performed using 2000–4000 water molecules. Since the canonical ensemble was used, the amount of water for each simulation was varied so that the pressure of the system was held constant across simulation runs. In all cases the average pressure was very close to 0 bar (± 0.1 kbar).

III. RESULTS

A. Water structure about polarizable cylinders: The influence of the dielectric constant

Before we analyze the interactions between polarizable cylinders in explicit water, let us consider the structure of water about a single cylinder as the polarizability of the cylinder is varied. The polarizability is adjusted by changing the value of the dielectric constant ϵ_{in} for the cylinder in Eq. (2). We have considered three cases: (i) a purely hydrophobic cylinder ($\epsilon_{in}=1$); (ii) a cylinder with dielectric permittivity ($\epsilon_{in}=2$), which is the typical value used in predictive macroscopic models of proteins;^{19,20} and (iii) a cylinder with a large dielectric permittivity on the high end of what may be used in modeling the active sites of biological molecules ($\epsilon_{in}=20$).^{20,21} We note that since the solvent is described explicitly, and, therefore $\epsilon_{out}=1$, when the cylinder has a dielectric constant larger than 1, the interaction between an external charge and its induced image on the cylinder surface is attractive.

The oxygen and hydrogen radial density profiles about the cylinder are shown in Fig. 2. The water penetrates the cylinder to a greater extent as the polarizability of the cylinder increases. For $\epsilon_{in}=2$ the cylinder is still hydrophobic, but for the largest polarizability, water layering as well as a high density contact layer of water at the surface occur. This indicates that for $\epsilon_{in}=20$ the cylinder is partially wetted by water. In essence, materials with a dielectric constant of the order of 20 already favor water solvation.

It is important to note that because of the charge neutrality condition imposed on the cylinder (see Sec. II), hydrogen and oxygen are both attracted (for $\epsilon_{in}>\epsilon_{out}$) to its surface because the induced charge is necessarily of both signs. This has a strong effect on the orientation of the water molecule near the cylinder surface. Thus the water dipoles preferentially align parallel or antiparallel to the radial vector ema-

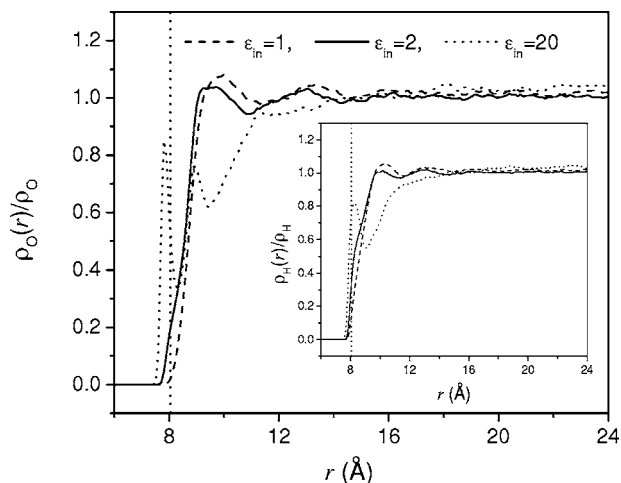


FIG. 2. Radial distribution functions of oxygen and hydrogen (inset) about cylinders of different dielectric constants. Increasing the polarizability (electrical permittivity) of the cylinders results in increased solvation of the cylinder. The vertical dotted line corresponds to the effective radius, the distance from the axis of the cylinder that a water molecule with a kinetic energy of $k_B T$ would penetrate the external potential [Eq. (1)], of the cylinder.

nating from the center of the cylinder. The orientation of the dipole moments of the water molecules about the cylinder can be quantified using the expression²²

$$P(r) = \left\langle \frac{\boldsymbol{\omega} \cdot \mathbf{r}}{|\boldsymbol{\omega}| |\mathbf{r}|} \right\rangle_r, \quad (3)$$

which is simply the statistical average of the projection of the water dipole moment orientation $\boldsymbol{\omega}$ (the vector from the oxygen atom site that perpendicularly bisects the line connecting the two hydrogen sites of the water molecule) in the radial direction at a radial distance r . A plot of $P(r)$ as a function of the radial location of the oxygen atom site of the water molecule about the cylinder is shown in Fig. 3. This figure shows the enhanced structure of water, specifically the

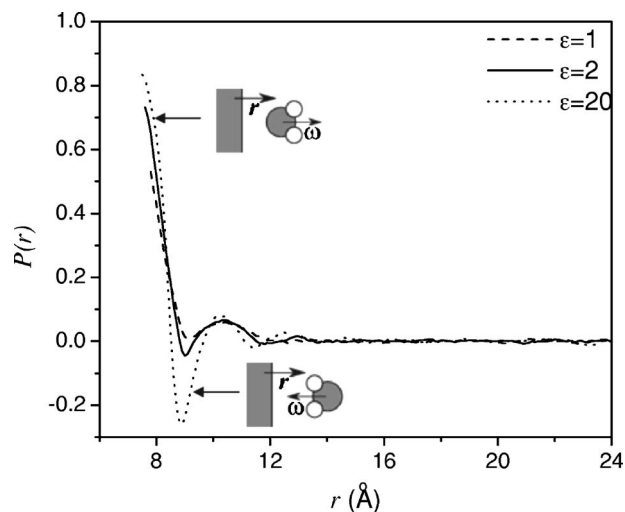


FIG. 3. The degree of orientation of water molecules about cylinders of increasing polarizabilities as a function of the location of the water's oxygen sites with respect to the center of the cylinder. Near the surface of the cylinder, the water dipole is oriented to a greater extent parallel or antiparallel to the radial direction vector.

increased alignment of the dipole orientation, about the cylinder as the polarizability of the cylinder is increased.

B. Forces between parallel polarizable cylinders in water

Now we turn to the polarizability-dependent interactions between two identical cylinders in parallel alignment. If we treat the solvent implicitly as a continuous dielectric medium, the only defined forces between the cylinders would be dispersion forces, i.e., charge fluctuation or van der Waals interactions, due to the cylinders having a different dielectric constant than that of the solvent.⁶

One such force arises from the attractive van der Waals, induced-dipole-induced-dipole, interaction between the individual atoms that make up the solutes. Using simple geometrical arguments and assuming additivity of the usual attractive r^{-6} van der Waals interaction of the atoms that compose each object, the force per unit length between two identical cylinders of radius R is given by⁶

$$F/l = \frac{AR^{1/2}}{16(D-2R)^{5/2}}, \quad (4)$$

where D is the interaxial distance between the cylinders and A is the Hamaker constant, which depends on the properties of the cylinders and the media within which they interact. In the Lifshitz theory of van der Waals forces, the Hamaker constant can be approximated by a form that only depends on the bulk properties of the media, namely, their dielectric constants and refractive indices.⁶ As an example, the Hamaker constant for the attractive force between two air bubbles in water, using only their known zero-frequency dielectric constants and refraction indices, is calculated to be 3.7×10^{-20} J.⁶

In our model, however, the object is not composed of individual atoms. The cylinder-cylinder interactions are the result of a very short-range, repulsive potential coupled with grid charges that interact via Coulomb forces. Hence, if the solvent was treated as a continuous medium, the only force would be that of the macroscopic induced-dipolar interactions between the cylinders.⁶ Following the derivation for the interaction between two dielectric spheres ($\epsilon = \epsilon_{in}$) suspended in water ($\epsilon = \epsilon_w \approx 80$) (Refs. 6 and 23) but now for the case of cylindrical solutes of radius R , the force per unit length on each cylinder is given by

$$F/l = -\frac{4k_B TR^4}{\lambda D^5} \left(\frac{\epsilon_{in} - \epsilon_w}{\epsilon_{in} + \epsilon_w} \right)^2, \quad (5)$$

where D , again, is the interaxial separation between the cylinders and λ corresponds to a decoupling length (≥ 1 Å), i.e., the approximate length for which the dipole moment rotating in the plane perpendicular to the long axis of the cylinder may change in both direction and magnitude along the length of the cylinder. This force is very short ranged but qualitatively predicts, e.g., the attraction between two microscopic air bubbles in a liquid.⁶

The utilization of an explicit solvent in the simulations, however, is expected to dramatically alter the short-range interactions between polarizable objects. As demonstrated in

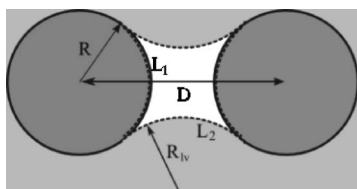


FIG. 4. The formation of a cavity of the solvent in the interstitial region between two cylindrical solutes.

the previous section, the structure of the solvent about the cylinders is heavily influenced by the degree of polarizability of the cylinders, which plays a central role in determining the interactions between the cylinders. Furthermore, a variety of other forces associated with an explicit solvent may manifest themselves in the interactions between the cylinders. When a solute is added to water, there is a free energy cost associated both with the restructuring of the solvent molecules about the solute (an entropic contribution) and a reduction in the attractive interactions between the solvent molecules near the surface of the solute (an energetic contribution). For a purely hydrophobic solute, the balance between the solute-solvent surface tensions favors the formation of a vapor layer between the solute and the liquid. This effect leads to “dewetting.”⁶ If two solutes are brought near each other, then, a vapor cavity arising out of the dewetting of each object, i.e., the formation of a liquid-vapor boundary parallel to the object’s surface, may form in the interstitial region between them to decrease the area of the energetically costly liquid-vapor interface.²⁴

Following a derivation similar to that carried out by Dzubiella and Hansen²² but for a cylindrical geometry, we can determine the conditions for cavity stability between two cylinders and also calculate the attractive force arising from this cavity formation. We consider first the difference in free energy per unit length l between a state where a cavity of cross-sectional area A_{cav} is formed between two cylinders separated by an interaxial distance D and a state where the cavity is filled with water. This free energy difference is approximately given by

$$\Delta\Omega/l \approx \Delta P A_{\text{cav}} - 2\gamma_e L_1 + 2\gamma L_2 + 2\gamma_{\text{cv}} L_1, \quad (6)$$

where L_i is the length of the interface i (see Fig. 4), γ_e is the surface tension of the liquid-cylinder interface, and γ is the surface tension of the water liquid-vapor interface. The final term in Eq. (6) may be neglected since the cylinder-vapor surface tension is much less than that of the other interfaces ($\gamma_{\text{cv}} \ll \gamma, \gamma_e$). Here, $\Delta P = P_l - P_v = \gamma/R_{lv}$ is the difference between the pressures of the liquid and of the vapor in the cavity arising from the finite curvature of the liquid-vapor interface, i.e., the Laplace pressure. To solve Eq. (6), we assume a contact angle π between the water and the cylinder, i.e., complete drying. The interfacial lengths appearing in Eq. (6) are given by $L_1 = 2R \arccos[D/(2(R+R_{lv}))]$ for the liquid-cylinder interface and $L_2 = 2R_{lv} \arcsin[D/(2(R+R_{lv}))]$ for the liquid-vapor interface of the cavity, which has a radius of curvature of R_{lv} (cf. Fig. 4). By minimizing the free energy [Eq. (6)] with respect to R_{lv} , we may determine the solute separations at which a cavity is stable, i.e., the free energy of

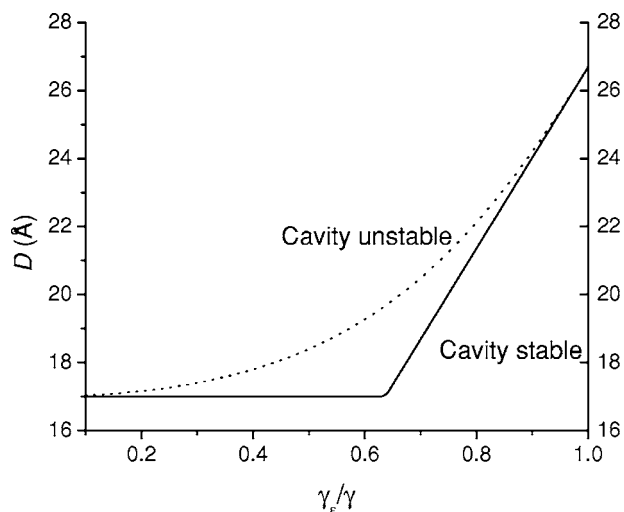


FIG. 5. The maximum interaxial separation at which cylinders of radius 8.5 Å can sustain a cavity between them as a function of the ratio of the surface tension of water at the liquid-cylinder interface and at the liquid-vapor interface. The solid line is the result of minimizing Eq. (6), and the dashed line is the result of minimizing this equation when the $\Delta P A_{\text{cav}}$ term is excluded.

the system with the cavity is less than that when the cavity is filled. In Fig. 5, the maximum interaxial distance between two cylinders of radius 8.5 Å where this cavity is stable is shown as a function of the ratio of the surface tension of the water liquid-cylinder and the water liquid-vapor interfaces. Also we represent in Fig. 5 the maximum interaxial distance for which the cavity is stable when the curvature term, $\Delta P A_{\text{cav}}$ in Eq. (6), is not included. One can see that this term has a dramatic effect, leading to a reduction in the separations at which the cavity remains stable. Nevertheless its effect is very small as $\gamma_e/\gamma \rightarrow 1$.

As shown in Fig. 5, decreasing the surface tension of the liquid-cylinder interface reduces the stability of the cavity. Next to a perfectly hydrophobic object, the surface tension is that of the liquid-vapor interface. But near a dielectric object, the surface tension between the object and the water is diminished—the electric field of induced charges of the dielectric object perturbs the structure of the water surface at the boundary. As the dielectric constant (effective polarizability) of the object increases, the surface tension between the water and the object decreases, enhancing the solvation of the polarizable material, as shown in Fig. 2. At low values of the dielectric constant, 1–2, however, a cavity can still be sustained. Furthermore, we find for the approximations taken above that the radius of curvature of the liquid-vapor interface for a stable cavity is essentially infinite so that the first term in Eq. (6) may be ignored when determining the force between the cylinders, and also, L_1 and L_2 then become, approximately, πR and D , respectively.

The force due to the cavity in between the two cylinders can be obtained by differentiating the minimized free energy with respect to the interaxial separation D ,

$$f/l = - \left. \frac{\partial(\Delta\Omega_{\text{min}}(D)/l)}{\partial D} \right|_T \approx -2\gamma. \quad (7)$$

The minimalistic thermodynamic model described above predicts that the force between the cylinders is zero for dis-

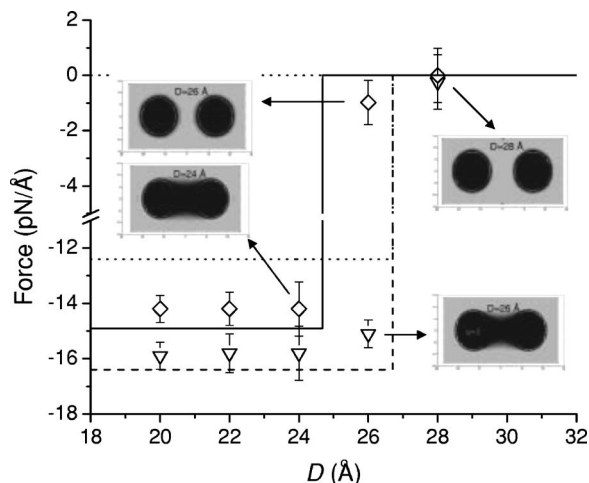


FIG. 6. The force per unit length between two cylinders when the cylinders have dielectric constants of $\epsilon_{in}=1$ (triangles) and $\epsilon_{in}=2$ (diamonds) for the explicit water simulations. (Note the break in the y axis.) The dotted line shows the contribution to the force only taking into account the surface tension term [Eq. (7)]. The dashed ($\epsilon_{in}=1$) and solid ($\epsilon_{in}=2$) lines correspond to the total forces when including the Laplace pressure term to account for the finite curvature of the liquid-vapor interfaces, as seen in the simulations. (These curves are shown assuming that the Laplace term remains constant with cylinder separation.) The insets show the density profile of water for the two cases at the separations just above and just below the points where the cavities collapse.

tances larger than the maximum interaxial separation for which the cylinders can sustain a cavity and -2γ for distances where the cavity exists.

The forces between two cylinders for two cases, where their dielectric constants are 1 (perfectly hydrophobic) and 2, are shown in Fig. 6. Our results are consistent with the behavior predicted by the thermodynamic models summarized by Eqs. (6) and (7). We observe the predicted discontinuity in the force at a specific cylinder-cylinder distance. Also, as predicted by the model (see Fig. 5), we find that the cavity collapses at a smaller separation for the $\epsilon_{in}=2$ cylinder as compared to that of the $\epsilon_{in}=1$ cylinder, which demonstrates that the surface tension at the liquid-cylinder interface is lower than the liquid-vapor value as the polarization of the cylinder increases. The points at which collapse of the cavity occurs for the two cases suggest that $\gamma_e \approx 0.9\gamma$ for the $\epsilon_{in}=2$ cylinder and $\gamma_e \approx \gamma$ for the $\epsilon_{in}=1$ cylinder (as expected). Again, the thermodynamic model above predicts an attractive “constant” force between the cylinders of $\sim -2\gamma$ when a cavity exists. The simulations show that indeed the force between the cylinders is essentially constant and of the order of -15 pN/Å. This value is rather close to the force expected using the model surface tension of the SPC/E water-air interface, -12.4 pN/Å.²⁵ This theoretical result [Eq. (7)] is also shown in Fig. 6.

We should emphasize that the theoretical force calculated above [Eq. (7)] was obtained by assuming that the liquid-vapor interface is flat. As observed in the insets of Fig. 6, however, the curvature of the interface appears to be finite. For $\epsilon=1$, considering the location of the liquid-vapor surface to be at the point where the density of water is half of its bulk value, we obtain $R_{lv} \sim 25$ Å at a separation of 26 Å. This curvature would engender an additional contribution to

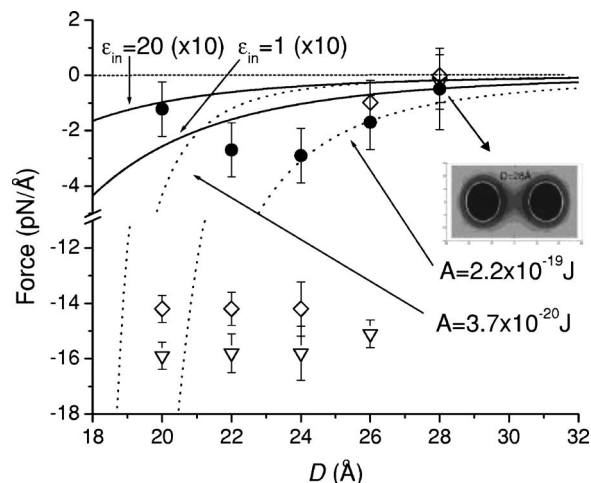


FIG. 7. The force per unit length between two cylinders when the cylinders have dielectric constants of $\epsilon_{in}=1$ (open triangles pointing down), $\epsilon_{in}=2$ (open diamonds), and $\epsilon_{in}=20$ (filled circles) for the explicit water simulations. The inset shows the density profile of water for the $\epsilon_{in}=20$ cylinders at an interaxial separation of 28 Å. The dotted curves correspond to the van der Waals force [Eq. (4)] associated with interactions between the atoms composing two dielectric cylinders interacting across the water for the Hamaker constants indicated. The solid curves (scaled by a factor of 10 for the sake of clarity) show the induced-dipole forces between macroscopic dielectric cylinders for two different dielectric constants [Eq. (5)]. Hence, the “dewetting” force is found to be much larger than that which may be attributed to continuum theories.

the attractive force of $\approx 2\gamma R/R_{lv} = 4$ pN/Å, which yields a total force that is consistent with that found from the simulations for $\epsilon_{in}=1$. Increasing the permittivity to $\epsilon_{in}=2$ results in a weaker force between cylinders, ~ -14 vs -16 pN/Å. This reduction in the force can also be explained in terms of the Laplace pressure since the radius of curvature is found to be larger, $R_{lv} \sim 40$ Å, and so will provide an additional ~ -2.5 pN/Å to the total force between the cylinders. Thus we note that the Laplace pressure term included in Eq. (6), which becomes dominant for macroscopic systems, adds a non-negligible contribution to the total force between objects of nanometer dimensions.

We would like to point out that the thermodynamic model discussed above and summarized in Eq. (6) is strictly valid only when there exists a vapor cavity between the polarizable objects. For systems with cylinders of $\epsilon_{in}=1$ and $\epsilon_{in}=2$, the average density of water in the interstitial region of the cylinders was found to be a fraction of a percent of the bulk value for cylinder separations where the large finite force was observed. Therefore the above thermodynamic model is applicable to both cases. Nevertheless this model has to be modified for situations where the solute-solvent interactions become increasingly attractive, as observed for the case with cylinders of $\epsilon_{in}=20$ discussed below, since increased interaction between the solute and solvent leads to kinetically unstable cavities.²⁶

Increasing the polarizability of the cylinder to $\epsilon_{in}=20$, we find that a cavity never forms. This is again consistent with the prediction of our simple thermodynamic model. Nevertheless, it is important to note that there still exists a net attractive force between the cylinders (see Fig. 7) that cannot be explained by this model. As shown in the inset of

Fig. 7, a finite density of water still exists between the cylinders due to the solvation of the cylinder (Fig. 2). But because there is a smaller water density in the interstitial region (approximately half that of the bulk value) as compared to the density on the opposite side of the cylinders, there is an asymmetry in the pressure of the water about the cylinder, leading to the attraction. At small separations, the attraction is observed to grow weaker. The confined geometry between the cylinders at these separations requires removing highly solvated water molecules from the cylinder surface, which is energetically unfavorable, thus adding a repulsive contribution to the total interaction. As a comparison, the van der Waals force between two cylinders [cf. Eq. (4)] for two different values of the Hamaker constant and the force due to induced-dipolar interactions between macroscopic cylinders, Eq. (5), are also shown. The van der Waals force is plotted for two representative values of the Hamaker constants corresponding to interactions across the water between two media with the dielectric properties of air and of semiconductors and metals.⁶ It is shown that the force induced by the solvent, either solvation forces ($\epsilon_{\text{in}}=20$) or surface tension forces (dewetting, $\epsilon_{\text{in}}=1, 2$), is of the same order of magnitude as the van der Waals force for intermediate distances. However, the solvation force is an order of magnitude larger than the force due to induced-dipolar interactions between macroscopic cylinders [Eq. (5)], making the latter contribution irrelevant in determining the interactions between the polarizable solutes. Overall our results indicate that the forces between nanometer scale dielectric media are *completely* dominated by capillary and solvation mediated forces.

IV. DISCUSSION AND FINAL REMARKS

A model for generic dielectric media, which can be easily implemented in molecular dynamics simulations, has been developed to consider the effects of explicit solvent on their interactions. Dielectric discontinuities have been replaced with an induced charge at the surface of the dielectric that is dependent on the free charge configuration, which includes the solvent contribution, of the system. Assuming that the media have an isotropic, linear dielectric response to external electric fields, increasing the polarizability of the dielectric media engenders simply changing the dielectric constant of the media. The finite polarizability of an object results in an attraction between the water partial charges and their induced charges. This attraction leads to an increased structure of the solvent around the polarizable object. This is reflected in both the density profiles and the average water dipole orientation, which aligns parallel/antiparallel to the radial axis of the cylinder. We find that an increase in the dielectric constant of the cylinder from $\epsilon_{\text{in}}=1-20$ is enough to modify the hydrophobic character of the cylinder.

For interactions between dielectric media in the explicit solution, the degree of polarizability of the media not only dictates the strength of the interaction but also the nature of the interaction. For hydrophobic media, $\epsilon_{\text{in}}=1$, the net force between the objects is dominated by a capillary interaction due to the overlap of the drying regions between the solutes.

This yields a very strong attraction since decreasing the separation of the objects results in a large reduction of the surface tension energy. As the polarizability of the solute increases, $\epsilon_{\text{in}}=2$, the effective surface tension between the solute and the surrounding water diminishes. This, in turn, decreases the range of the capillary force because the cavity formed due to dewetting becomes less energetically favorable. Finally, objects with large dielectric constants, $\epsilon_{\text{in}}=20$, become solvated, and consequently the capillary contribution to the force is absent. Nevertheless, attraction between polarizable solutes persists due to the structural changes in the solvent about the solute. The solvation force is of the same order of magnitude as the force expected from van der Waals interactions between two cylinders in water. This solvation force, however, cannot be described using macroscopic models that consider polarizable media in a solvent modeled as a dielectric continuum. Overall our results indicate that the phase separation of solutes in water should heavily depend on the polarizability of the solute.

In this work we have considered polarizable solutes in water. Nonetheless our model can be readily extended to study interactions in other polarizable media, such as ionic solutions.²⁷ As with interactions between polarizable media themselves, the forces between ions and dielectric media will be contingent on the polarizability of the media as well as on the solvation energies of the ions. Finally, this dielectric model could be used in conjunction with charged sites to study interactions of large molecules, e.g., proteins and DNA, where fully atomistic simulations are not required.

ACKNOWLEDGMENTS

Financial support from the Royal Society is acknowledged by one of the authors (A.W.) and funding from EPSRC is gratefully acknowledged by another author (F.B.). Some of the simulations were carried out on the HPCx supercomputer through the Materials Chemistry Consortium and on the Viking Linux cluster maintained by London e-Science Centre.

APPENDIX: DERIVATION OF THE INDUCED SURFACE CHARGE ON A DIELECTRIC CYLINDER DUE TO AN EXTERNAL POINT CHARGE

In cylindrical coordinates, the potential due to a point charge q at \mathbf{r}' in vacuum can be written as an expansion of modified Bessel functions²⁸

$$\psi_{\text{ext}}(\mathbf{r}) = \frac{q}{4\pi\epsilon_0|\mathbf{r}-\mathbf{r}'|} \equiv \frac{q}{2\pi^2\epsilon_0} \sum_{m=-\infty}^{\infty} e^{im(\varphi-\varphi')} \times \int_0^{\infty} dk \cos[k(z-z')] I_m(kr_{<}) K_m(kr_{>}). \quad (\text{A1})$$

When this charge is placed near a dielectric cylinder, the potential will be modified both inside and outside the cylinder due to the charge's field-induced polarization of the bound charge within the cylinder. This new potential may be found by using the conditions that the potential and the normal component of the displacement field must be continuous across the lateral cylinder boundary.

First, invoking superposition, we can write the total potential everywhere as the sum of the potential due to the point charge and that of the induced charge on the cylinder,

$$\psi(\mathbf{r}) = \psi_{\text{ext}}(\mathbf{r}) + \psi_{\text{ind}}(\mathbf{r}), \quad (\text{A2})$$

where $\psi_{\text{ind}}(\mathbf{r})$, which satisfies Laplace's equation, can be written in the general forms¹³

$$\begin{aligned} \psi_{\text{ind}}(r < R_c) \\ = \frac{q}{2\pi^2\epsilon_0} \sum_{m=-\infty}^{\infty} e^{im\phi} \int_0^{\infty} dk \cos(kz) \Psi_m(k) I_m(kr), \end{aligned} \quad (\text{A3a})$$

$$\begin{aligned} \psi_{\text{ind}}(r > R_c) \\ = \frac{q}{2\pi^2\epsilon_0} \sum_{m=-\infty}^{\infty} e^{im\phi} \int_0^{\infty} dk \cos(kz) \Phi_m(k) K_m(kr). \end{aligned} \quad (\text{A3b})$$

These forms of the expansion guarantee that the potential is well behaved at the origin and at infinity. Applying the boundary conditions at the surface of the cylinder, we can solve for the unknown functions $\Psi_m(k)$ and $\Phi_m(k)$. This yields a potential due to an induced charge located at $(r' = d (d > R_c), \phi' = 0, z' = 0)$ inside the cylinder of

$$\psi_{\text{ind}}(r, \phi, z) = \frac{(\kappa - 1)q}{2\pi^2\epsilon_{\text{out}}} \sum_{m=-\infty}^{\infty} e^{im\phi} \int_0^{\infty} dk \frac{I'_m(kR_c) I_m(kr) K_m(kR_c) K_m(kd) \cos(kz)}{[I_m(kR_c) K'_m(kR_c) - \kappa I'_m(kR_c) K_m(kR_c)]}. \quad (\text{A4})$$

The induced charge then can be found using

$$\boldsymbol{\sigma}_{\text{ind}}(\mathbf{r}_{\text{sur}}) = \mathbf{P}(\mathbf{r}) \cdot \hat{\mathbf{n}} = -\epsilon_0 \chi (\nabla \psi(\mathbf{r})|_{r=r_{\text{sur}}}) \cdot \hat{\mathbf{r}}, \quad (\text{A5})$$

where $\mathbf{r}_{\text{sur}} = (R_c, \phi, z)$ is the location of the induced charge on the cylinder surface and $\hat{\mathbf{r}}$ is the unit radial vector. Summing Eqs. (A1) and (A4) to find the total potential inside the cylinder and substituting this into Eq. (A5), we obtain Eq. (2) in the text. In practice, it was found that the value for the potential, Eq. (A4), converged upon summing the azimuthal angle index, m , up to a value of 70 for the positions of the external charge considered.

¹R. R. Netz and J.-F. Joanny, *Macromolecules* **32**, 9013 (1999); R. R. Netz, *J. Phys.: Condens. Matter* **15**, S239 (2003).

²H. H. von Grunberg and E. C. Mbamala, *J. Phys.: Condens. Matter* **12**, 10349 (2000); **13**, 4801 (2001).

³G. Iversen, Y. I. Kharkats, and J. Ulstrup, *Mol. Phys.* **94**, 297 (1998), and references therein.

⁴D. Bratko, B. Jonsson, and H. Wennerstrom, *Chem. Phys. Lett.* **128**, 449 (1986).

⁵L. B. Boinovich and A. M. Emelyanenko, *Adv. Colloid Interface Sci.* **104**, 93 (2003).

⁶J. Israelachvili, *Intermolecular and Surface Forces*, 2nd ed. (Academic, London, 1991).

⁷J. Faraudo and F. Bresme, *Phys. Rev. Lett.* **92**, 236102 (2004); **94**, 077802 (2005).

⁸J. Tomasi and M. Persico, *Chem. Rev. (Washington, D.C.)* **94**, 2027 (1994); C. J. Cramer and D. G. Truhlar, *ibid.* **99**, 2161 (1999).

⁹H. Hoshi, M. Sakurai, Y. Inoue, and R. Chujo, *J. Chem. Phys.* **87**, 1107 (1987).

¹⁰D. Boda, D. Gillespie, W. Nonner, D. Henderson, and B. Eisenberg, *Phys. Rev. E* **69**, 046702 (2004).

¹¹R. Allen, J.-P. Hansen, and S. Melchionna, *Phys. Chem. Chem. Phys.* **3**, 4177 (2001).

¹²A. A. Kornyshev and S. Leikin, *J. Chem. Phys.* **107**, 3656 (1997).

¹³W. R. Smythe, *Static and Dynamic Electricity* (McGraw-Hill, New York, 1939).

¹⁴A. Wallqvist, *Chem. Phys. Lett.* **165**, 437 (1990).

¹⁵A. Kohlmeier, W. Witschel, and E. Spohr, *Chem. Phys.* **213**, 211 (1996).

¹⁶I.-C. Yeh and M. L. Berkowitz, *J. Chem. Phys.* **112**, 10491 (2000).

¹⁷K. A. Motakabbir and M. L. Berkowitz, *Chem. Phys. Lett.* **176**, 61 (1991).

¹⁸F. Bresme and J. Faraudo, *Langmuir* **20**, 5127 (2004).

¹⁹T. Simonson and C. L. Brooks III, *J. Am. Chem. Soc.* **118**, 8452 (1996).

²⁰C. N. Schutz and A. Warshel, *Proteins* **44**, 400 (2001).

²¹G. King, F. S. Lee, and A. Warshel, *J. Chem. Phys.* **95**, 4366 (1991).

²²J. Dzubiella and J.-P. Hansen, *J. Chem. Phys.* **121**, 5514 (2004).

²³L. D. Landau, E. M. Lifshitz, and L. P. Pitaevskii, *Electrodynamics of Continuous Media*, 2nd ed. (Butterworth-Heinemann, Oxford, 1984), Vol. 8.

²⁴K. Lum, D. Chandler, and J. D. Weeks, *J. Phys. Chem. B* **103**, 4570 (1999).

²⁵We have performed computer simulations of a water slab in order to compute the surface tension of the interface. We find that the surface tension of the SPC/E model (using a cutoff of 17 Å for the short-range interactions) at 298 K is 62 mN/m. This surface tension results in a force per unit length of $f/l = -12.4$ pN/Å.

²⁶A. Luzar, *J. Phys. Chem. B* **108**, 19859 (2004).

²⁷F. Bresme and A. Wynveen (unpublished).

²⁸J. D. Jackson, *Classical Electrodynamics*, 3rd ed. (Wiley, New York, 1999).